GENERALIZED BILINEAR MODEL BASED NONLINEAR UNMIXING USING SEMI-NONNEGATIVE MATRIX FACTORIZATION

Naoto Yokoya,[1] *Jocelyn Chanussot,*[2] *and Akira Iwasaki*[3]

[1]Department of Aeronautics and Astronautics, The University of Tokyo, Japan
[2]GIPSA-lab, Signal and Image Dept., Grenoble Institute of Technology, Grenoble, France
[3]Research Center for Advanced Science and Technology, The University of Tokyo, Japan

ABSTRACT

Nonlinear spectral mixing models have recently been receiving attention in hyperspectral image processing. This work presents a novel optimization method for nonlinear unmixing based on a generalized bilinear model (GBM), which considers second-order scattering effects. Semi-nonnegative matrix factorization is used for optimization to process a whole image in a matrix form. The proposed method is applied to an airborne hyperspectral image with many endmembers and shows good performance both in unmixing quality and computational cost with simple implementation. The effect of endmember extraction on nonlinear unmixing is investigated and the impact of the nonlinearity on abundance maps is demonstrated.

***Index Terms*—** hyperspectral image, nonlinear unmixing, generalized bilinear model, semi-nonnegative matrix factorization

1. INTRODUCTION

Spectral unmixing is an important task for hyperspectral (HS) image interpretation. Many researchers have worked on this problem with a linear mixture model (LMM) that assumes that an observed spectrum is a linear combination of several endmember spectra. The LMM is a simplified spectral mixture model that considers only first-order scattered photons by neglecting multiple photon interactions. Although LMM based unmixing methods can retrieve physically meaningful results, nonlinearity in spectral mixture model is pointed out by some works [1]-[4]. In recent years, nonlinear unmixing for HS images is receiving attention in remote sensing image exploitation. Nonlinear spectral mixing occurs due to multiple reflection and transmission from surface [2]. The bilinear mixture model (BMM), which considers second-order scattering of photons between two distinct materials, has been studied by several groups [5]-[7]. The generalized bilinear model (GBM) introduces an effective means to deal with the underlying assumptions in the BMM [7]. The GBM method was applied to small images of synthetic and real HS data with three endmembers [7, 8]. When applied to larger images in an unsupervised manner with many endmembers, the optimization process becomes more challenging.

In this work, we present a novel optimization method for the GBM and apply it to a real HS image with many endmembers. The effect of endmember extraction on nonlinear unmixing is investigated and the impact of the second-order scattering effects on abundance maps is visualized.

2. GBM UNMIXING VIA SEMI-NONNEGATIVE MATRIX FACTORIZATION

2.1. Generalized bilinear model

The BMM takes account of second-order photon interactions between different D endmembers as additional terms in the LMM assuming that third or higher order interactions are negligible [4]. In the BMM, the observed L-spectrum of a single pixel $\mathbf{y} \in \mathbb{R}^{L\times 1}$ is given by:

$$\mathbf{y} = \mathbf{E}\mathbf{a} + \sum_{i=1}^{D-1}\sum_{j=i+1}^{D} b_{i,j}\mathbf{e}_i \odot \mathbf{e}_j + \mathbf{n}, \tag{1}$$

where $\mathbf{E} \in \mathbb{R}^{L\times D}$ is the endmember matrix with the *i* th column vector $\mathbf{e}_i \in \mathbb{R}^{L\times 1}$ representing the *i* th endmember spectrum, $\mathbf{a} \in \mathbb{R}^{D\times 1}$ is the abundance vector, $b_{i,j}$ is the interaction abundance between the *i* th and *j* th endmembers, $\odot$ is the Hadamard (element-wise product) operation, and $\mathbf{n} \in \mathbb{R}^{L\times 1}$ is the additive noise. On the right side, the first term denotes the linear mixing and the second term represents the second-order interaction, which is assumed to be a linear combination of bilinear endmember spectra, i.e., the bilinear mixing. From a physical perspective, the GBM introduces the nonlinear mixing coefficient $c_{i,j}$ as $b_{i,j} = c_{i,j}a_i a_j$ and assumes the following constraints:

$$\begin{aligned} &a_i \geq 0 \ \ \forall i \in 1,...,D \ \text{ and } \ \sum_{i=1}^{D} a_i = 1, \\ &0 \leq c_{i,j} \leq 1 \ \ \forall i \in 1,...,D-1 \ \ \forall j \in i+1,...,D. \end{aligned} \tag{2}$$

When the endmembers are known, the GBM unmixing turns to the optimization of the abundance (**a**) and the interaction coefficient (**c**) under the constraints of (2). Several optimization methods are proposed in [8].

2.2. Semi-nonnegative matrix factorization for GBM

In this work, the new optimization method based on semi-nonnegative matrix factorization (Semi-NMF) is introduced to speed up the optimization process of a whole image in a matrix form. The observed HS image can be reshaped as a matrix form $\mathbf{Y} \in \mathbb{R}^{L\times P}$ with P representing the number of pixels. The BMM for the whole image is given in a matrix form by

$$\mathbf{Y} = \mathbf{EA} + \mathbf{MB} + \mathbf{N} \tag{3}$$

where $\mathbf{A} \in \mathbb{R}^{D\times P}$ is the abundance matrix, $\mathbf{M} \in \mathbb{R}^{L\times D(D-1)/2}$ is the bilinear endmember matrix, $\mathbf{B} \in \mathbb{R}^{D(D-1)/2\times P}$ is the interaction abundance matrix, and $\mathbf{N} \in \mathbb{R}^{L\times P}$ is the noise matrix. The GBM unmixing becomes the following minimization with respect to **A** and **B**:

$$\text{minimize} \quad \|\mathbf{Y} - \mathbf{EA} - \mathbf{MB}\|_F^2 \tag{4}$$

$$\text{subject to} \quad \mathbf{A} \succeq 0, \quad \sum_{i=1}^{D} A_{i,k} = 1, \quad 0 \preceq \mathbf{B} \preceq \mathbf{A}^* \tag{5}$$

where $A^*_{(i,j),k} = A_{i,k}A_{j,k} \quad (\forall k \in 1, ..., P)$ and the operator $\|\cdot\|_F$ denotes the Frobenius norm. By introducing $\mathbf{Y}_1 = \mathbf{Y} - \mathbf{MB}$ and $\mathbf{Y}_2 = \mathbf{Y} - \mathbf{EA}$, (3) is written as follows

$$\mathbf{Y}_1 = \mathbf{EA} + \mathbf{N}, \tag{6}$$

$$\mathbf{Y}_2 = \mathbf{MB} + \mathbf{N}. \tag{7}$$

Separately minimizing $\|\mathbf{Y}_1 - \mathbf{EA}\|_F^2$ and $\|\mathbf{Y}_2 - \mathbf{MB}\|_F^2$ can be an approximation of the solution of the original problem (4) performed by an alternating optimization algorithm. Owing to physical constraints, all components of **E**, **M**, **A**, and **B** are nonnegative. Therefore, the minimization of (4) can be solved by Semi-NMF that factorizes a non-restricted matrix **X** into a non-restricted matrix **F** and a nonnegative matrix $\mathbf{G}^T$ as $\mathbf{X} \approx \mathbf{FG}^T$ [9]. Semi-NMF optimization is guaranteed to converge to a local optimum with the alternative update rules. With **E** given and **M** calculated from **E**, the GBM unmixing is solved by the following update rules for **A** and **B**:

$$\mathbf{A}^T \leftarrow \mathbf{A}^T .* \sqrt{((\mathbf{Y}_1^T\mathbf{E})^+ + \mathbf{A}^T(\mathbf{E}^T\mathbf{E})^-)./((\mathbf{Y}_1^T\mathbf{E})^- + \mathbf{A}^T(\mathbf{E}^T\mathbf{E})^+)} \tag{8}$$

$$\mathbf{B}^T \leftarrow \mathbf{B}^T .* \sqrt{((\mathbf{Y}_2^T\mathbf{M})^+ + \mathbf{B}^T(\mathbf{M}^T\mathbf{M})^-)./((\mathbf{Y}_2^T\mathbf{M})^- + \mathbf{B}^T(\mathbf{M}^T\mathbf{M})^+)} \tag{9}$$

where $.*$ and $./$ denote elementwise multiplication and division. $(\mathbf{C})^+$ and $(\mathbf{C})^-$ are the positive and negative parts of a matrix **C** defined as $\mathbf{C}^+ = (|\mathbf{C}| + \mathbf{C})/2$, $\mathbf{C}^- = (|\mathbf{C}| - \mathbf{C})/2$. The GBM unmixing via Semi-NMF is as follows.

Algorithm: Generalized bilinear model based nonlinear unmixing via Semi-NMF

Input: Hyperspectral data $\mathbf{Y} \in \mathbb{R}^{L\times P}$ and endmember matrix $\mathbf{E} \in \mathbb{R}^{L\times D}$.
Output: Abundance matrix $\mathbf{A} \in \mathbb{R}^{D\times P}$ and interaction abundance matrix $\mathbf{B} \in \mathbb{R}^{D(D-1)/2\times P}$.
Step 1: **A** is initialized by the fully constrained least square (FCLS) method [10] based on the LMM.
Step 2: $\mathbf{A}^*$ is calculated and **B** is set as $\delta \times \mathbf{A}^*$ with small value of δ.
Step 3: **A** and **B** are alternately updated by (8) and (9). If any element of **B** exceeds that of $\mathbf{A}^*$, it is replaced by that of $\mathbf{A}^*$. To satisfy the abundance sum-to-one constraint, the method from [10] is adopted.

3. EXPERIMENT

The GBM via Semi-NMF is applied to an airborne HS data taken over vegetation because multiple scattering is a common phenomenon in vegetation areas [1]-[4]. The dataset was acquired by a Compact Airborne Spectrographic Imager 3 (CASI-3) taken over pasture area in Hokkaido, Japan, on June 19, 2009. We selected a 150×150 pixel size image with 68 spectral channels over 410-1070 nm and 1 m ground sampling distance (GSD). The data initially measured as radiance were converted into reflectance.

Vertex component analysis (VCA) [11], which is one of the most common convex-geometry-based endmember extraction methods with the pure pixel assumption, is used for endmember extraction. The performance of the proposed method is numerically evaluated by the reconstruction error (RE), the spectral angle mapper (SAM), and the computational time comparing with FCLS and the gradient descent algorithm (GDA), which showed good results for the GBM unmixing applied to a real HS image in [8]. RE and SAM are commonly used to evaluate the performance of the unmixing procedure for real datasets. They are calculated using the observed ($\mathbf{y}_k$) and estimated ($\hat{\mathbf{y}}_k$) spectra as follows:

$$\text{RE} = \sqrt{\frac{1}{LP}\sum_{k=1}^{P}\|\hat{\mathbf{y}}_k - \mathbf{y}_k\|^2}, \tag{10}$$

$$\text{SAM} = \frac{1}{P}\sum_{k=1}^{P}\arccos\left(\frac{\mathbf{y}_k \cdot \hat{\mathbf{y}}_k}{\|\mathbf{y}_k\|\|\hat{\mathbf{y}}_k\|}\right). \tag{11}$$

By changing the number of endmembers extracted by VCA, we examined the second-order interaction term and the residual errors of the GBM. The impact of these values at a single pixel is calculated by root-sum-square (RSS). After the endmember extraction, the abundance maps and the impact of bilinear mixing on these abundance maps are estimated.

4. RESULTS AND DISCUSSION

Table 1 shows the comparison of the RE and SAM values, and the computational cost relative to different four numbers

Table 1. Comparison of RE ($\times 10^{-3}$) and SAM (in degree) values, and computational costs (in sec).

	$D = 6$			$D = 11$			$D = 16$			$D = 21$		
	RE	SAM	Time	RE	SAM	Time	RE	SAM	Time	RE	SAM	Time
FCLS	10.562	2.695	**20.5**	6.320	1.824	**57.4**	5.025	1.488	**95.2**	4.738	1.433	**143.5**
GDA	10.548	2.692	122.2	6.318	1.823	223.1	5.048	**1.479**	670.6	4.721	1.431	785.7
Semi-NMF	**10.264**	**2.640**	55.4	**6.258**	**1.816**	106.6	**4.975**	1.483	169.7	**4.701**	**1.429**	250.4

of endmembers, i.e., $D = 6, 11, 16, 21$. The CPU used is Intel(R) Core(TM) i7 CPU 2.80 GHz, with a memory capacity of 16 GB. The Semi-NMF method shows the best performance in RE and SAM for many cases of the number of endmembers. In addition, the computational time is smaller than GDA. Especially, even when the number of endmembers becomes large, the Semi-NMF method converges to good local optima with reasonable computational cost owing to the simple update rules in a matrix form. This result indicates that Semi-NMF is a good candidate for the optimization of the GBM unmixing regarding its convergence and easy implementation.

Fig. 1 shows the RSS maps of the second-order interaction term and the unmixing residual errors. As the number of endmembers increases (6, 11, 16, and 21), the two maps converge. We concluded 16 is enough for the number of endmembers. In spite of the large number of endmembers, the bilinear mixing effect clearly appears in areas B and C in Fig. 1, i.e., the boundary between grass and tree, and the narrow path. With $D = 6$, area A in Fig. 1 corresponding to grass shows the high bilinear effect but the residual error still remains high in this area. It significantly decreases after the grass is detected as the endmember with $D = 11$. It means the endmember extraction has larger influence on the residual errors of unmixing than the bilinear mixing effect. Therefore, to discuss the nonlinear mixing, the accurate endmember extraction is the major premise.

Since VCA is sensitive to the outlier, it detects some endmembers that are only present in very specific regions. To visualize the abundance map and the bilinear mixing effect, we manually eliminated such kind of specific endmembers and re-processed the GBM unmixing with 10 endmembers as shown in Fig. 2 (a). In Fig. 2 (b), the colored circles indicate the locations of these endmembers, with each color corresponding to that of spectrum in Fig. 2 (a). The endmembers are labeled by visual judgment considering the locations of endmembers and comparing the abundance maps and the RGB color image. Fig. 2 (c) and (d) show the abundance maps for these ten materials and their differences with the LMM, which demonstrate the impacts of the second-order interaction on the abundance maps. In some regions, the abundance fractions changed more than 2% from the LMM because of the multiple scattering effect.

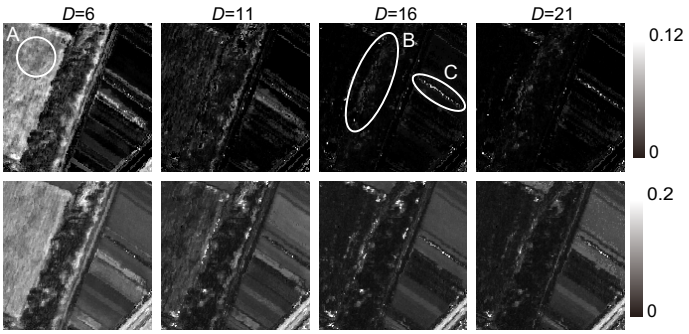

Fig. 1. RSS maps of second-order interaction terms (top) and unmixing residual errors (bottom).

5. CONCLUSION

This work presented a novel optimization method based on Semi-NMF for the GBM unmixing and demonstrated its application to an airborne real HS image taken over a vegetation scene with many endmembers. Semi-NMF enables the optimization of the GBM unmixing for processing a whole image in a matrix form, with simple update rules. The proposed method showed useful results both in unmixing quality and computational cost. By examining the effect of endmember extraction on nonlinear unmixing, the residual errors of unmixing are more influenced by the endmember extraction than the bilinear spectral mixing effect. The impact of the second-order scattering effects on abundance maps is visualized. With accurate endmember extraction, Semi-NMF based GBM has a possibility to deal with spectrally complex HS images, thereby contributing to the practical use of nonlinear unmixing.

6. ACKNOWLEDGMENT

The authors would like to thank Prof. J. Tourneret for providing the GDA code. This project is partly carried out under the contracted with AIST (National Institute of Advanced Industrial Science and Technology).

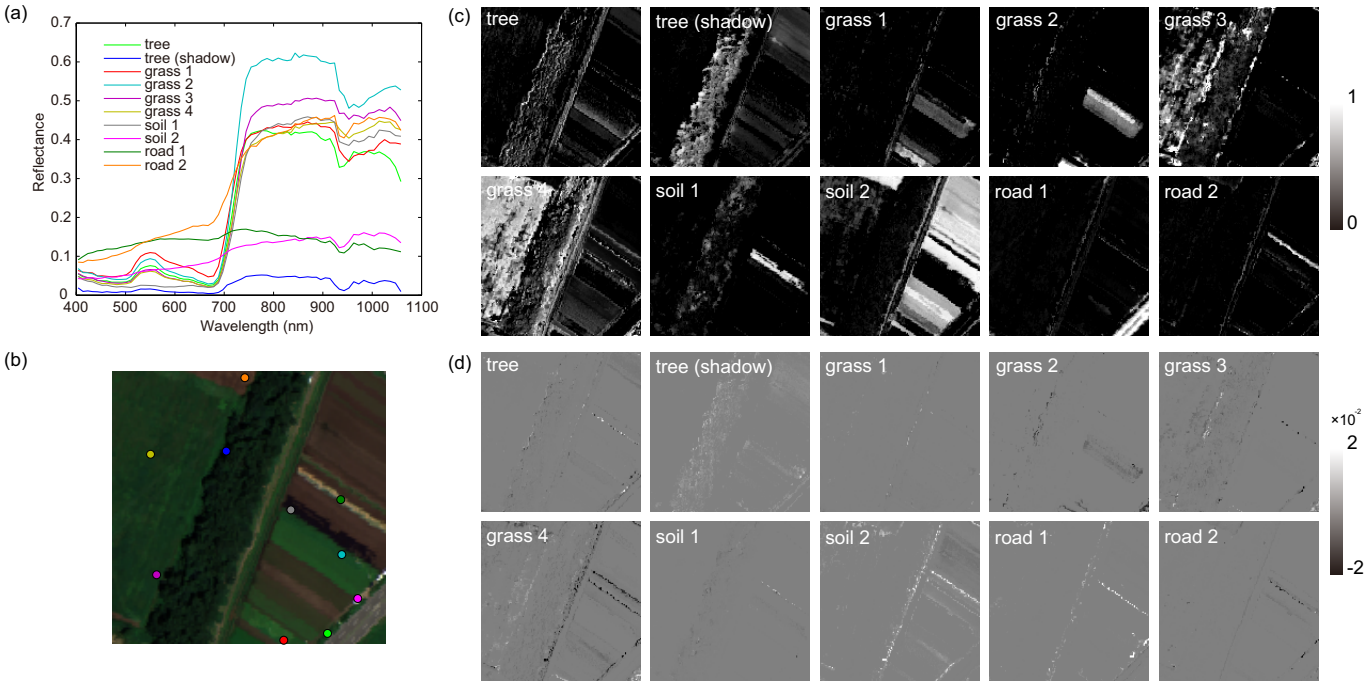

Fig. 2. (a) Endmember spectra, (b) location of endmembers, (c) abundance maps, and (d) differences of abundance maps with LMM.

7. REFERENCES

[1] D.A. Roberts, M.O. Smith, and J.B. Adams, "Green vegetation, nonphotosynthetic vegetation, and soils in AVIRIS data," *Remote Sens. Environ.*, vol. 44, pp. 117–126, 1993.

[2] C. C. Borel and S. A. W. Gerstl, "Nonlinear spectral mixing models for vegetative and soil surfaces," *Remote Sens. Environ.*, vol. 47, pp. 403–416, 1994.

[3] L. Zhang, D. Li, Q. Tong, and L. Zheng, "Study of the spectral mixture model of soil and vegetation in PoYang Lake area, China," *Int. J. Remote Sens.*, vol. 19, no. 11, pp. 2077–2084, 1998.

[4] B. Somers, K. Cools, S. Delalieux, J. Stuckens, D. V. der Zande, W. W. Verstraeten, and P. Coppin, "Nonlinear hyperspectral mixture analysis for tree cover estimates in orchards," *Remote Sens. Environ.*, vol. 113, no. 6, pp. 1183–1193, Jun. 2009.

[5] W. Fan, B. Hu, J. Miller, and M. Li, "Comparative study between a new nonlinear model and common linear model for analysing laboratory simulated-forest hyperspectral data," *Int. J. Remote Sens.*, vol. 30, no. 11, pp. 2951–2962, Jun. 2009.

[6] J. M. Nascimento and J. M. Bioucas-Dias, "Nonlinear mixture model for hyperspectral unmixing," in *Proc. SPIE*, 2009, vol. 7477, p. 74770I.

[7] A. Halimi, Y. Altmann, N. Dobigeon, and J. Tourneret, "Nonlinear unmixing of hyperspectral images using a generalized bilinear model," *IEEE Trans. Geosci. Remote Sens.*, vol. 49, no. 11, pp. 4153–4162, Nov. 2011.

[8] A. Halimi, Y. Altmann, N. Dobigeon, and J. Tourneret, "Unmixing hyperspectral images using the generalized bilinear model," *IEEE IGARSS*, pp. 1886–1889, 2011.

[9] C. Ding, T. Li, and M. I. Jordan, "Convex and semi-nonnegative matrix factorization," *IEEE Trans. Patten Anal. Mach. Intell.*, vol. 32, no. 1, pp. 45–55, 2010.

[10] D. C. Heinz and C.-I. Chang, "Fully constrained least squares linear spectral mixture analysis method for material quantification in hyperspectral imagery," *IEEE Trans. Geosci. Remote Sens.*, vol. 39, no. 3, pp. 529–545, Mar. 2001.

[11] J. M. Nascimento and J. M. Bioucas-Dias, "Vertex component analysis: A fast algorithm to unmix hyperspectral data," *IEEE Trans. Geosci. Remote Sens.*, vol. 43, no. 4, pp. 898–910, Apr. 2005.